Exploiting thermoplasmonic effects for laser-assisted preparation of Au nanoparticles/InZnO thin film with visible range photodetection properties

Ching-fu Lin, Amine Khitous, Hsiao-wen Zan, Olivier Soppera

Exploiting thermoplasmonic effects for laser-assisted preparation of Au nanoparticles/InZnO thin film with visible range photodetection properties

Ching-Fu Lin[1,2,3,4], Amine Khitous,[1,2] Hsiao-Wen Zan[3,4], Olivier Soppera[1,2]

[1.] *Université de Haute-Alsace, CNRS, IS2M UMR 7361, F-68100 Mulhouse, France*

[2.] *Université de Strasbourg, France*[3.]

[3] *Department of Photonics and Institute of Electro-Optical Engineering, College of Electrical and Computer Engineering, National Yang Ming Chiao Tung University, Hsinchu, 300, Taiwan, ROC*

[4] *Department of Photonics and Institute of Electro-Optical Engineering, College of Electrical and Computer Engineering, National Chiao Tung University, Hsinchu, 300, Taiwan, ROC*

Abstract:

We propose a new method for preparing gold nanoparticles (Au NPs)/indium-zinc-oxide (IZO) nanocomposite thin films based on photothermal mechanisms with near-Infrared (NIR) laser-annealing, which allows integrating the nanomaterial on fragile substrates such as thin glass, plastic sheets, or 3D printed pieces. The Au NPs were first prepared by NIR laser dewetting of a thin Au layer. Then, the Au NPs were used to locally cure the semiconductor material and provide suitable electronic properties owing to their efficient thermoplasmonic effects under our NIR laser annealing conditions. Finally, the electronic properties of the Au NPs/IZO thin films were characterized in the dark and under light excitation. Good photoresponsivity at 410 nm (UV, > 10^0 A/W) was demonstrated, but interestingly, the presence of Au NPs significantly improved the detection ability to a longer wavelength range, such as to 515 nm (green, ~ 5×10^{-3} A/W), even extending to 630 nm (red, ~ 5×10^{-4} A/W), and 780 nm (NIR, ~ 10^{-4} A/W). In addition, with the critical evaluation of dynamic light detection and lifetime trace (> 22 days), the laser-annealed Au NPs/IZO photodetector (PD) demonstrated useful operating reliability and stability.

1. Introduction

Over the past few decades, thin-film oxide semiconductor devices have attracted considerable interest for various applications **[1]**, such as nanogenerators **[2]**, sensors for biomedical **[3]** or gas detection **[4]**, photomemories **[5,6]**, and photodetectors (PDs) **[7,8]**. To achieve such excellent electrical properties, thin-film deposition by a high-vacuum system, such as sputtering, have been widely used **[9–11]**. Such processes usually require high cost for device fabrication. In contrast, the use of solution-based materials, especially for metal precursors used in sol-gel chemistry, has attracted significant interest over the past few years **[12–17]**. To achieve a thin-film oxide material based on the sol-gel method, a high-temperature thermal annealing process is usually necessary. It is necessary to remove the organic ligands and promote the condensation reaction to obtain a metal-oxide thin film from a xerogel structure. However, high-temperature treatment may limit further applications on flexible or plastic substrates. To date, a few techniques have been reported to overcome these drawbacks. Deep ultraviolet (DUV) or near infrared (NIR) annealing have already been proposed as the critical step for fabricating thin-film oxide semiconductor devices. Kim et al. **[18]**, Bolat et al. **[19]**, and Moon et al. **[20]** showed that DUV or NIR annealing at low environmental temperatures can be successfully used to obtain thin-film devices with good carrier mobility and electrical properties. Furthermore, we recently showed that the use of NIR dyes can significantly improve the NIR laser curing of sol-gel indium-zinc-oxide (IZO) materials and allow their use as gas sensors **[21]**.

One of the key parameters for the laser curing of metal-oxide precursors is to generate high absorption and efficient conversion to thermal energy. Because the sol-gel layers have an intrinsic low absorption in the NIR, it is necessary to add absorbers in the thin film to generate a local temperature increase. Highly conjugated organic molecules (NIR dyes), carbon black, and carbon nanotubes are potential candidates. Gold nanoparticles (Au NPs) have also proved their utility. Under light excitation, significant thermal effects can be generated, which are known as thermoplasmonic effects **[22–27]**. They correspond to the damping of a plasmon resonance, which creates a temperature increase at the surface of NP that depends on several parameters such as irradiance of the incident light, irradiated area, light wavelength, nature and morphology, surface density, nature of the surrounding medium, and the substrate **[28]**. In specific conditions, temperature increases such as

several hundreds of degrees are achievable and have been used to trigger several chemical reactions **[29–31]**. In this paper, we demonstrate that this route is suitable for curing IZO thin films.

Moreover, when Au is used as nanoheaters in the film, the final material comprises Au NPs embedded in a MO thin film, which can be interesting for applications, such as PDs, with a sensitivity range that can span the UV and visible ranges owing to the extinction spectra of Au NPs. We demonstrated the potential of our process through the proof-of-concept fabrication of a PD. Because visible-light detection **[32,33]** is interesting for biomedical detectors or colorimetric sensors in the Internet of Things (IoT), UV PDs **[34]** are important for chemical and biological analysis or flame detection and NIR PD **[35,36]** opens new possibilities in optical imaging for brain science, medical diagnostics, or remote sensing. Therefore, designing a PD under a low environmental temperature fabrication process with a wide range of detection ability and good operating lifetime without an extra encapsulation process is crucial. Herein, we aim to provide a fabrication process that is compatible with these features and with substrates that cannot withstand thermal annealing, even at moderate temperatures for such PDs.

In this study, a PD with a wide detection range was successfully prepared from sol-gel IZO with Au NPs by full NIR laser annealing. ZnO was chosen because it is an environmentally friendly material **[37]** with a wide energy band gap (~ 3.3 eV) and stability in air. Its carrier mobility can be easily adjusted by ion doping, like indium ion doping, which is commonly used in thin-film transistors (TFTs) **[38]**. To fabricate ZnO-based PDs with an improvement in photoresponse of the long wavelength range, NIR laser annealing was first used to generate Au NPs by laser-induced dewetting of Au thin film **[39]**. This method was chosen because it can be performed at room temperature, and it is a convenient way to generate dense arrays of Au NPs. Indeed, the localized surface plasmon resonance (LSPR) effect generated from Au NP nanostructures coupled to IZO can extend the photosensitivity toward the visible range and NIR **[40,41]**. Furthermore, we discovered that using Au NPs as nanoheaters by low-power light excitation, we were able to ensure the curing of the thin-film semiconducting material by thermoplasmonic effects **[42,43]**. This novel approach allowed the preparation of Au NPs covered by an IZO thin layer with a wide range of light-detecting properties. The fabrication process is detailed, and we demonstrated

the central role of the Au NPs in the fabrication process and the final photodetecting properties.

Finally, examples of Au NPs/IZO PDs were successfully fabricated on 3D printable polymer sheets, which firmly indicated that the novel NIR laser annealing technique can contribute to a breakthrough approach for integrating optoelectronic functions in the field of 3D printing technology.

2. Experimental section

2.1 Materials

Indium nitrate (indium(III) nitrate hydrate, 99.9%), zinc nitrate (zinc nitrate hexahydrate, ≥99.0%), and 2-methoxyethanol (2-MOE, ≥99.9%), which were used for forming photosensitive layer by sol-gel synthesis method, were purchased from Sigma Aldrich. The Au target for forming Au thin films (NPs) was purchased from Eloïse (France).

2.2 Synthesis of IZO using the sol-gel process:

To prepare the sol-gel IZO solution, indium nitrate and zinc nitrate precursors were dissolved in 2-MOE at a molar ratio of 5:4. The total concentration of indium: zinc in the solution was 0.25 M. After stirring for 24 h, the solution was used in the following PD fabrication steps.

2.3 Fabrication process of Au NPs/IZO PDs

Fig. 1(a) illustrates the fabrication steps for forming Au NPs/IZO PDs by an 808-nm-laser-annealing. The laser source was a high-power array of VCSELs (Innoptics) providing a maximum of 60 W over surfaces adjustable from 5 × 5 to 20 × 20 cm^2. Initially, the substrates were prepared by a standard cleaning process, including dipping them in acetone and ethanol with ultrasonic baths. Next, the substrates were deposited in a sputtering machine (CRESSINGTON 108 auto) to form an Au film with a nominal thickness of 8 nm. The first laser-annealing step was used to generate Au NPs with no additional treatment.

The IZO precursor solution was deposited by spin-coating (SÜSS MicroTec spin-coater), thereby resulting in a continuous layer of IZO precursors covering the Au NPs. Then, a 2^{nd} laser-annealing process was adopted to convert the IZO

precursors into amorphous IZO by removing solvent and organic residues, and inducing condensation. Finally, 20-nm-Au electrodes were deposited by sputtering through a shadow mask, which defined the active area of the PD as $2 \times 2\ mm^2$. **Fig. 1(b)** shows a schematic of the cross-section structure of the PD. The interval between the electrodes was set to 200 μm, which helped the device work as a miniaturized photosensitive resistor. In addition, **Fig. 1(c)** shows a real image of the experimental sample fabricated by an 808-nm-laser-annealing, including the Au NPs synthesized by the 1st annealing process (28 $W \cdot cm^{-2}$ for 30 min) and Au NPs with IZO curing by the 2nd annealing process (20 $W \cdot cm^{-2}$ for 1 h). As seen in these images, the generation of Au NPs by the 1st laser annealing results in a color change from the olive to purple. After IZO was coated on the Au NPs during the 2nd annealing process, the color of the treated part changed again to indigo.

For the comparison of Au NPs/IZO PDs fabricated by conventional thermal and the novel 808-nm-laser-annealing process, one PD with a similar structure was prepared. The fabrication process was the same as that in **Fig. 1(a)**, except that the 1st and 2nd annealing processes were replaced by the thermal annealing processes. In all cases, the Au NPs arrays were characterized by UV-vis spectroscopy. With given fabrication process parameters, good reproducibility could be obtained, as proved by reproducible extinction spectra.

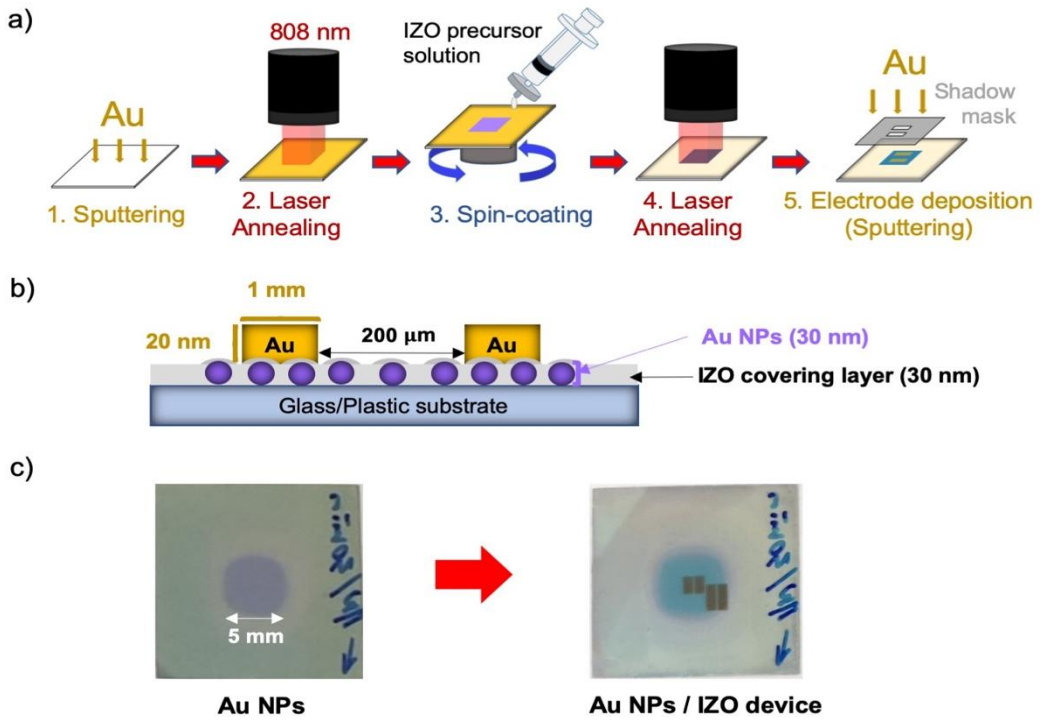

Fig. 1: (a) Schematic of the PDs fabrication process. (b) Cross-section structure of the PD device. (c) Full laser-processed Au NPs doped IZO PD as in steps 3 and 5 of the fabrication process.

2.4 Device characterization

Atomic force microscopy (AFM) was performed using a Molecular Imaging PicoPlus (resonant mode). Au NP morphology was also studied by TEM with an ARM200F JEOL high-resolution transmission electron microscope. Silicon TEM grids with two rectangular slits (1500 × 100 μm) covered one face, with a 50 nm-thick Si_3N_4 membrane (TEDPELLA). UV-visible spectra were recorded on a PerkinElmer Lambda 950 spectrophotometer, and XPS spectra were recorded on a ULVAC-PHI, PHI QuanteraII.

The light detection performance of the Au NPs/IZO PD was evaluated at 410 nm (UV), 465 nm (blue), 515 nm (green), and 630 nm (red) using commercial LEDs, and at 780 nm with an NIR laser diode. In addition, the PDs were connected to the electrical measurement system (KEITHLEY 2636B) to provide the sweeping voltage or fixed bias voltage with a dynamic monitoring function to collect the electrical properties.

3. Results and discussion

3.1. Surface morphology and LSPR characteristics of Au NPs/IZO film

In this study, Au NPs served as the key components of the device for their fabrication and final properties. The spectral properties of the PD are directly linked to the LSPR of the NPs, which are driven by their morphology. The synthesis of Au NPs on glass substrates was thus optimized. **Fig. 2(a)–2(c)** show the surface morphology obtained by AFM. **Fig. 2(a)** shows the original Au film with a thickness of 8 nm, with a smooth surface morphology (roughness: 1.27 nm). In **Fig. 2(b)**, the sample was synthesized by a thermal annealing process (300 °C, 1 h). As shown in **Fig. 2(c)**, the sample was synthesized by an 808-nm-laser-annealing process (28 $W \cdot cm^{-2}$, 30 min). Both exhibited a discontinuous structure on their surfaces, demonstrating Au NPs can be synthesized by either thermal or laser treatment. In addition, the morphology of the Au NPs synthesized by laser-annealing process (average thickness: 29.6 nm, under 28 $W \cdot cm^{-2}$, 30 min) could be tuned to similar

results as those synthesized by the thermal annealing process (average thickness: 23.6 nm, under 300 °C, 1 h). For confirming the exact size distribution of Au NPs, TEM was used. **Fig. 2(d)** shows the image of Au NPs obtained by thermal annealing under the same conditions as **Fig. 2(b)**, wherein well-disconnected Au NPs can be observed. The average distance between NPs appears to be more important in TEM analysis, which can be explained by the AFM tip aspect ratio in AFM images that artificially decrease this distance. Furthermore, from the TEM image analysis, the mean perimeter [**Fig. S1(a)**] and mean area [**Fig. S1(b)**] can be evaluated, which helps in evaluating the average diameter of Au NPs as approximately 21.9 nm (assuming a circular shape, which is a rough estimation). Interestingly, the NP structure remained unchanged after IZO coating (**Fig. S1(c) to S1(e),** average diameter: 20.2 nm). For all preparation conditions used in this study, it can be observed that the size and morphology of NPs is quite inhomogeneous. As shown later in this paper, such characteristic generates a broad extinction spectrum that is very interesting for fabricating PDs with broad spectral sensitivity.

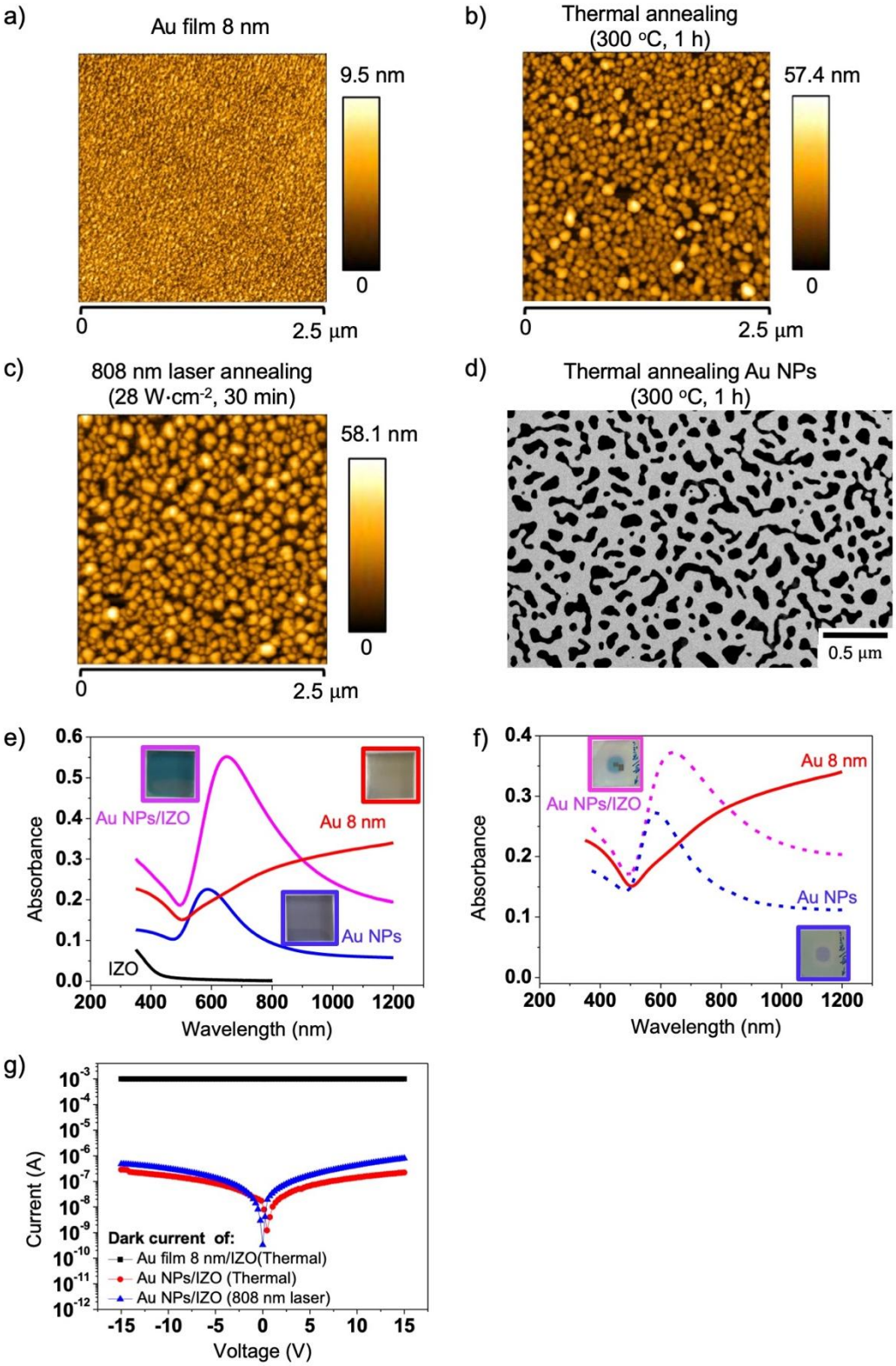

Fig. 2: AFM images of (a) Au film (8 nm), (b) Au NPs synthesized by 300 °C thermal-annealing for 1 h, and (c) Au NPs synthesized by an 808 nm laser annealing at 28 $W \cdot cm^{-2}$ for 30 min. (d) TEM images of Au NPs synthesized by 300 °C thermal-annealing for 1 h; the absorption spectra of each corresponding fabrication process of Au NPs/IZO structure (e) by thermal-annealing (Au NPs (300 °C, 1 h)/IZO (400 °C,

1 h), and (f) by laser-annealing (Au NPs (28 W·cm^{-2}, 30 min)/IZO (20 W·cm^{-2}, 1 h)). (g) The electrical characteristic comparison of devices prepared by thermal annealed IZO (400 °C, 1 h) covered with Au film or Au NPs (300 °C, 1 h) and laser annealed Au NPs (28 W·cm^{-2}, 30 min)/IZO (20 W·cm^{-2}, 1 h) film.

To further investigate the correlation between the 808-nm-laser-annealing and thermal annealing process, **Fig. 2(e)** and **2(f)** display the corresponding NP extinction spectra, which cover the range from 350 (UV) to 1200 nm (IR) for each fabrication step. From **Fig. 2(e)**, the original spectrum of the 8-nm-Au film (red curve) shows absorption in the entire light spectrum from 350 to 1200 nm. Although the Au film can have stronger absorption in the NIR range, no obvious absorbing peak can be observed. After the 1st thermal annealing process (300 °C, 1 h) for Au NP synthesis, an absorption peak at 586 nm (blue curve) can be observed owing to the LSPR effect. The spectral position of this peak is related to the average size **[44]**. The IZO film has an extremely weak absorption in the visible or NIR wavelength ranges (**Fig. 2(e),** black curve), which justifies the coupling of IZO with Au NPs. After the 2nd annealing process (400 °C, 1 h), the extinction spectrum of Au NPs is red-shifted to 650 nm (purple curve). This is mainly owing to the increase in the effective refractive index of the medium surrounding the Au NPs. Indeed, it is well established that the refractive index of sol-gel layers increases during thermal treatment owing to the loss of organic functions and densification induced by condensation reactions, resulting in the shift of LSPR **[45]**. The absorption in the NIR range of the raw Au film with a thickness of 8 nm suggests that a photothermal treatment may be possible using NIR laser annealing (808 nm continuous laser) to replace the conventional thermal annealing process. **Fig. 2(f)** shows the spectra of Au NPs prepared by the 808-nm-laser-annealing process. The results are similar to those obtained by thermal treatment; the generation of Au NPs by the 1st laser-annealing process (28 W·cm^{2}, 30 min) produces a peak at 580 nm (blue curve). These results confirm the data obtained by AFM showing that continuous NIR laser annealing can produce metal NPs. This approach is beneficial because the second annealing step can also be conducted using the same laser. After IZO covering and 2nd laser annealing (20 W·cm^{-2}, 1 h), the heat generated by the Au NPs is sufficient to red-shift the absorption peak to 645 nm (purple curve), which is close to the value obtained by thermal treatment.

To confirm the formation of disconnected Au NPs, the electrical properties of the thin films were characterized. **Fig. 2(g)** shows the dark current measured from the devices of an 8-nm-Au film coated with IZO (Au film/IZO) and IZO with Au NPs coupling (Au NPs/IZO) under an 808 nm laser or thermal annealing process. For the Au film, a high current was recorded (approximately 10^{-3} A), which can be explained by the shortcut produced by the continuous Au film under the IZO layer. For Au NPs/IZO, the conductivity can be successfully lowered and the current reached around 10^{-7} A. This result confirms the discontinuous structure of Au NPs and confirms the similar structures that can be obtained by both thermal and laser annealing.

3.2 Correlation of an 808 nm laser or thermal-annealed IZO with chemical analysis:

The curing of IZO under laser annealing was investigated by XPS and TEM. **Fig. 3(a)** and **3(b)** show the XPS analysis of the O(1s) peak for the Au NPs/IZO film fabricated by full thermal or 808-nm-laser-annealing. For each annealing process, we compared the results before and after IZO curing on glass substrates with Au NPs. In **Fig. 3(a)**, the changes observed under thermal annealing are consistent with those reported previously **[21]**. A significant decrease in vacancies was observed with an increase in the M-O, which corresponds to the condensation reactions induced by thermal treatments. The moderate temperature leads to amorphous materials, which explain the relatively high level of vacancies in the final material. Remarkably, **Fig. 3(b)** shows a similar structure of the O(1s) peak after IZO curing by an 808-nm-laser-annealing under 20 $W \cdot cm^{-2}$, 1 h. This confirms the possibility of using Au NPs as nanoheaters with a temperature increase that is sufficient to obtain the same material as thermal curing at 400 °C. Photoplasmonic effects have been the subject of extensive experimental and numerical studies recently **[46–49]**, and we confirmed here that it can be used very efficiently to generate local heating to promote chemical reactions. The effect is quite efficient under our conditions owing to the choice of NIR wavelength for irradiation, and the high density of NP at the surface, which promotes collective effects.

Furthermore, XPS confirms the structure of the Au NPs/IZO film, as schematized in **Fig. 1(b)** because the Au signal cannot be found from full range XPS scanning for

each sample (**Fig. S2(a)** and **S2(b)**). This shows that the IZO layer fully covers the Au NPs and is also confirmed by chemical mapping of the Au NPs/IZO film achieved by TEM analysis (**Fig. 3(c)**). On these images, the homogeneous distribution of Zn and In within the thin film is also demonstrated.

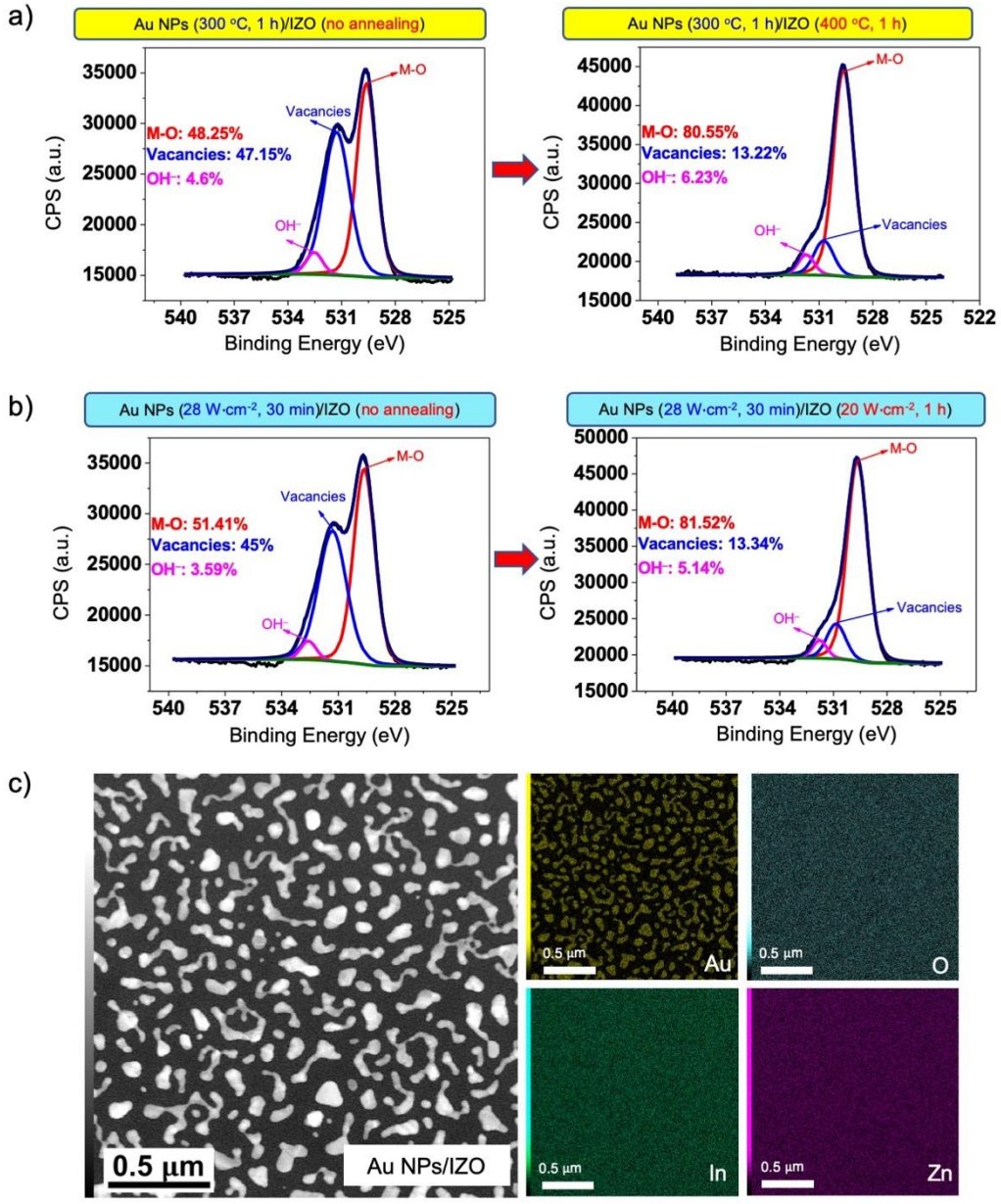

Fig. 3: XPS analysis for IZO before/after (a) thermal annealing (400 °C, 1 h) or (b) an 808 nm laser annealing (20 W·cm^{-2}, 1 h) on glass substrates with Au NPs; (c) The chemical mapping of thermal annealed Au NPs (300 °C, 1 h)/IZO (400 °C, 1 h) film.

3.3 Light-detecting performance of an 808-nm-laser-annealed Au NPs/IZO PD:

The light detection performance of Au NPs/IZO PDs was evaluated to demonstrate that these devices can serve as broadband PDs. Thermal-annealed IZO (400 °C, 1 h) PDs were used as reference devices for comparison with the devices prepared with an 808-nm-laser-annealing (1st annealing: 28 W/cm^2, 30 min, and 2nd annealing: 20 W·cm^{-2}, 1 h). In addition, commercial LEDs with illumination peaks at 410 nm (UV, 38 mW·cm^{-2}), 465 nm (blue, 750 mW·cm^{-2}), 515 nm (green, 325 mW·cm^{-2}), 630 nm (red, 325 mW·cm^{-2}), and 780 nm laser diode (NIR, 275 mW·cm^{-2}) were used in this section.

Fig. 4(a) shows the dark and light-induced (blue and red LEDs) current for the thermally annealed IZO (without Au NPs) and laser-annealed Au NPs/IZO PDs. From the results, both PDs have similar dark current levels, which implies that the IZO film fabricated under two different annealing treatments can have similar carrier mobilities. It also shows that when Au NPs are discontinued, they do not contribute significantly to the sample conductivity. For blue light detection, the response is quite similar for devices with and without NPs. For longer wavelength detection, such as red light detection, the IZO PD was found with little light detection performance. However, with the assisting absorption of Au NPs, the detection of red light (red curves) is significantly improved when using laser-annealed Au NPs/IZO PDs. Apart from the light-detecting performance shown on **Fig. 4(a)**, **Fig. S3(a)** to **S3(g)** offer the compilations of an 808-nm-laser-annealed Au NPs/IZO PD with keeping the 1st annealing condition as 28 W·cm^{-2} for 30 min, but adjusting the 2nd annealing power from 16 to 24 W·cm^{-2}, and increasing the treatment time from 10 to 60 min. To summarize the trend, the dark current level can be increased from 10^{-8} to 10^{-4} A by increasing the laser-annealing power and time. However, the higher dark current level can finally lead to the extinction of light-detecting ability because the difference between photo-induced and dark current cannot be well distinguished anymore.

To further point out the role of Au NPs, the normalized photoresponsivity calculated by the following function (1) **[50]** for both the thermally annealed IZO and laser-annealed Au-NP-doped IZO PDs are shown in **Fig. 4(b)** and **4(c)**. Because the PDs in our work were designed as photosensitive resistors, the photoresponsivity can exhibit symmetric performance by sweeping voltage measurements.

$$\text{Photoresponsivity} = \frac{{I_{light} - I_{dark}}/{Area\ of\ PD}}{{Power\ of\ light\ source}/{Area\ of\ light\ source}}. \quad (1)$$

From **Fig. 4(b)**, the thermally annealed IZO PD can perform good photoresponsivity for the range in UV (>10^0 A/W, 410 nm), and available photoresponsivity in the visible range, such as blue (~ 2×10^{-2} A·W^{-1}, 465 nm) and green (~ 5×10^{-4} A·W^{-1}, 515 nm) with the bias voltage at 15 V. However, from the photoresponsivity of the laser-annealed Au NPs/IZO PD in **Fig. 4(c)**, it not only keeps similar results for UV and blue light detection as shown in **Fig. 4(b)**, but also has a better performance for green (~ 5×10^{-3} A·W^{-1}, 515 nm) light detection, even contributes to the light-detecting ability in the range of red (~ 5×10^{-4} A·W^{-1}, 630 nm) and NIR (~10^{-4} A·W^{-1}, 780 nm). Moreover, the calibration curves of photoresponsivity to wavelength of light converted from **Fig. 4(c)** are shown in **Fig. 4(d)**. From **Fig. 4(d)**, the increasing trend of photoresponsivity mainly follows the increasing power of incident photons from 780 to 410 nm. Because the results measured under a higher bias voltage can have better photoresponsivity, a bias voltage of 15 V was selected for dynamic light detection analysis.

Fig. 4(e) shows the dynamic light detection performance of the laser-annealed Au NP/IZO PD. With repeated light irradiation (1 min) and recovery (6 min) for three rounds, almost all the light-induced responses, which are defined by the value of the current difference (ΔI) between the photo-induced current and dark current, can easily be found. Although the laser-annealed PD can already perform reliable light-detecting signals, on the other hand, the slow recovery time may come from the carrier persisting phenomenon **[6]** in IZO or the carrier blocking effect by the Schottky barrier in the Au/IZO surface **[41]**.

To evaluate the operating stability of an 808-nm-laser-annealed Au NPs/IZO PD, **Fig. 4(f)** offers its lifetime tracing performance by collecting light-induced (green and red LEDs) and dark current. From the results, the dark and light-induced current can almost be maintained at the same level in nearly 1 month (> 22 d), and the operation stability of the PD can be determined.

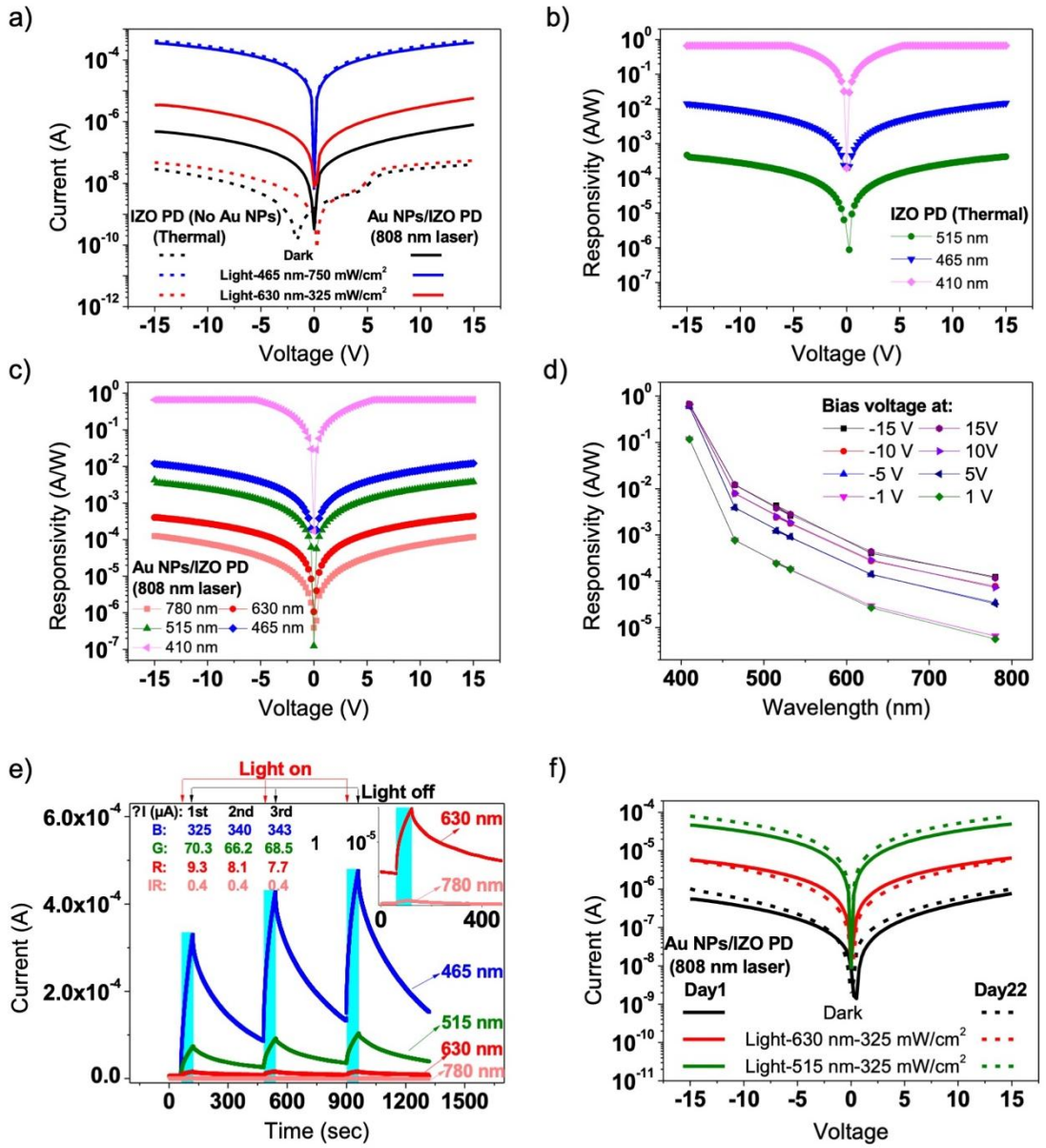

Fig. 4: The discussion based on electrical properties with an 808 nm laser annealed Au NPs (28 W·cm^{-2}, 30 min)/IZO (20 W·cm^{-2}, 1 h) PD and thermal annealed IZO (400 °C, 1 h) PD (a) the comparison of light/dark current performance; the photoresponsivity of (b) thermal annealed IZO, (c) an 808 nm laser annealed Au NPs/IZO PD; (d) the calibration relation of 808 nm laser annealed Au NPs/IZO PD with different operating bias voltage (e) the dynamic light-detecting performance, and (f) the lifetime tracing performance of an 808 nm laser annealed Au NPs/IZO PD

The photodetection properties demonstrated by this nanocomposite material prepared by laser annealing are thus comparable with other thermal annealing processes described in the literature **(Table.1)**. Although organic **[51,52]**

donor-acceptor (D-A) hybrid devices can be easily fabricated under a low-temperature process (80–120 °C), and demonstrate good photoresponsivity from visible to NIR (460–800 nm) range, it is still challenging to maintain UV sensing or good lifetime performance without encapsulation to avoid oxidation from water or oxygen. Organic perovskite-inorganic hybrid PDs **[53,54]** have been designed for improving the photoresponsivity in the visible range, but storing the devices without encapsulation in a glove box with inert gas can still be necessary for extending the device operating lifetime (~ 80 d) **[53]**. In addition, inorganic quantum dot (QD) based **[55,56]** or dye-sensitized oxide semiconductor **[57]** PDs offer excellent wide-range detection performance from the UV to NIR (410–1130 nm) range, especially for inorganic QDs doped PDs, can maintain a good lifetime (~ 160 d) **[55]** without encapsulation in ambient air. However, the high temperature annealing process (200–500 °C) may not be neglected in consideration of these studies. Based on the comparison above, each kind of thermal annealed PD has its own target to achieve specific light-detecting characteristics. However, with the aim of lowering down the device fabrication cost, an encapsulation-free Au NPs/IZO PD prepared by 808 nm laser annealing has been successfully proposed in this work, including low temperature process for device fabrication with good photosensitivity from UV to NIR and long operation lifetime. The encapsulation-free design also enhances the possibility for further applications on flexible surfaces.

Nanocomposite material	Processing temperature (°C)	Range for light detection (nm)	Maximum photoresponsivity ($A \cdot W^{-1}$)	Operation lifetime (Day)
Organic donor-acceptor (D-A) hybrid **[51,52]**	80-120	460-800	~10^{-2} (at 500, 650, 800 nm)	--
Organic perovskite-inorganic hybrid **[53,54]**	105-150	380-740	~10^{-1} (at 380, 450, 550, 630, 740 nm)	80 (glove box) **[53]**
Inorganic quantum dot (QD) **[55,56]** Dye-sensitized oxide semiconductor **[57]**	200-500	410-1130	>10^{1} (at 410 nm) ~10^{3} (at 465 nm) ~10^{2} (at 520 nm) ~10^{3} (at 635 nm) ~10^{-1} (at 1130 nm)	~160 (air) **[55]**
Au NPs/IZO (this work)	**NIR laser process at room temperature**	**410-780**	**>10^{1} (at 410 nm) ~10^{-2} (at 465 nm) ~10^{-3} (at 515 nm) ~10^{-4} (at 630, 780 nm)**	**>22 (air)**

Table.1: The comparison with alternative nanocomposite PDs

3.4 Light-detecting mechanism of an 808-nm-laser-annealed Au NPs/IZO PD:

To realize the wide range (410–780 nm) light-detecting performance of our

808-nm-laser-annealed Au NPs/IZO PD, the inclusion of Au NPs is expected to play the most significant role. From Haifei et al. **[58]** with the mechanism shown in **Fig. 5(a)**, when the wavelength of incident light corresponds to the LSPR range of Au NPs, it can be absorbed by the NPs. Next, the charge distribution for forming dipoles in Au NPs **[59]** can be found, and the oscillation direction of plasmonic damping follows the amplitude direction of the incident electromagnetic wave. Afterwards, the energy of the surface scattering phenomenon, which comes from a part of plasmonic damping, can finally lead to the generation of hot electrons on the surface of Au NPs. Therefore, the hot electron transfer phenomenon happening at the interface of the M-O contact can dominate the light-induced current in the long wavelength range.

Due to the use of five light sources in total to compare the photoresponsivity of thermally annealed IZO and an 808-nm-laser-annealed Au NPs/IZO PDs (**Fig. 4(b)** and **(c)**), **Fig. 5(b)** to **5(e)** are the corresponding band diagrams for discussing the light-detecting mechanism. For 410 nm (UV) detection in **Fig. 5(b)**, both of the 2 PDs can have similar and the best performance. This is mainly because the photon energy of 410 nm (~ 3.03 eV) is quite close to the band gap of IZO, leading to band to band excitation of carriers in IZO. When the irradiation wavelength of light becomes longer to 465 nm (blue), the photoresponsivity of **Fig. 4(b)** and **4(c)** can still maintain almost consistent performance. Owing to the absorption decrease of IZO, the defect levels that exist in between valance (E_v) and conduction (E_c) band can provide assistance for light-induced carrier excitation. When the irradiation light is shifted to 515 nm (green), the different photoresponsivity of the two PDs can be observed. Although the IZO PD can still work for this light detection, the photoresponsivity of Au NPs/IZO PDs can be 10× higher, which proves the importance of Au NPs coupling. From **Fig. 5(d)**, the defect levels in IZO can still work for generating photo-induced carriers; however, the hot electrons transferred from the Au NPs to IZO offer another route for forming light-induced current. Owing to the hot electrons generated from the LSPR effect on Au NPs, the temporary Fermi–Dirac distribution of hot electrons can be built, which finally results in the contribution of photo-induced current by thermionic emission. Finally, **Fig. 5(e)** corresponds to the detection of an extremely long wavelength range, such as 630 nm (red) and 780 nm (NIR). Because the IZO PD hardly demonstrates its photoresponsivity in this range, the Au NPs/IZO PD can still have the available detection ability, the hot electron transfer of Au NPs plays the most significant role in

this detection. To conclude, both IZO and Au NPs/IZO PDs can be used for UV and visible (blue and green) light detection. However, the assistance of Au NPs doping can eventually extend the light detection range to red, even to NIR, to achieve the target of wide-range detection.

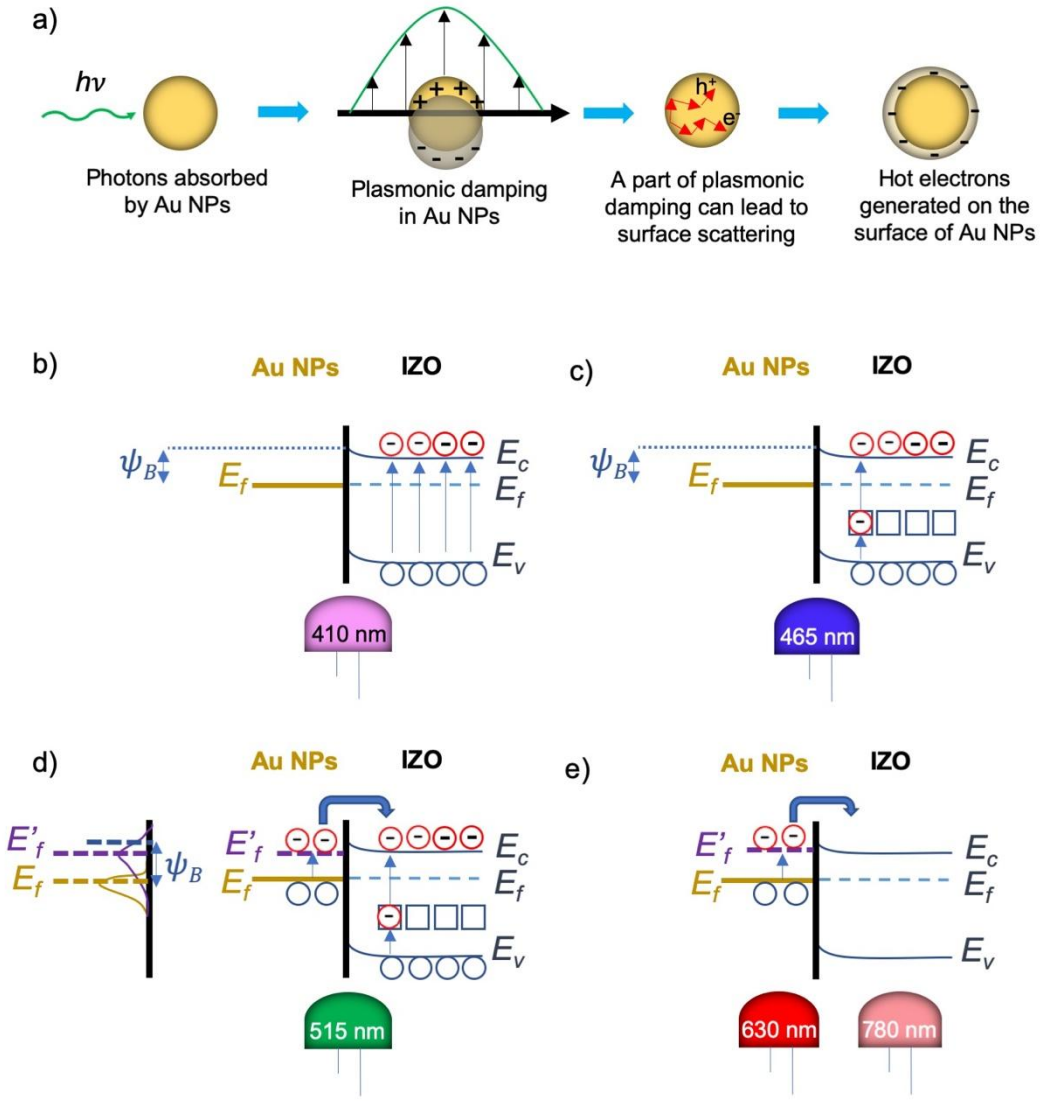

Fig. 5: (a)The generation steps of hot electrons on Au NPs, and the light-detecting mechanism base on M-O contact with (b) 410 nm-UV, (c) 465 nm-blue, (d) 515 nm-green, and (e) 630 nm-red and 780 nm-NIR

3.5 An 808-nm-laser-annealed Au NPs/IZO PD on plastic/flexible substrates:

In this last section, we demonstrate one of the most interesting features of our new fabrication process. To extend the field of applications, we produced some examples of full laser-processed Au NPs/IZO PDs on 3D polymer pieces (Dentona

Optiprint Splint 385) substrates prepared by 3D printing. Owing to the tolerance of heat on such substrates cannot be as high as glass substrates, the low power of the 808-nm-laser-annealing process for both Au NPs synthesis and IZO curing is necessary. **Fig. 6(a)** shows the AFM image of Au NPs synthesized from 8 nm Au film by the 808-nm-laser-annealing process (5.5 $W \cdot cm^{-2}$, 10 min). Compared to the Au NPs on glass substrates, the obviously different topographies can be predicted by the different interactions between the Au/substrates and the lower power laser-annealing process. After the 2nd annealing (5 $W \cdot cm^{-2}$, 10 min) step for IZO coupling, the UV light (365 nm, 81.1 $mW \cdot cm^{-2}$) detection performance is shown in **Fig. 6(b)**. From **Fig. 6(b)**, the Au NPs/IZO PD can be used to demonstrate UV detection because the repeated ΔI value can be collected. Although the light-detecting performance still needs to be improved, the useful applications of Au NPs/IZO PDs on arbitrary 3D printed figures can be expected.

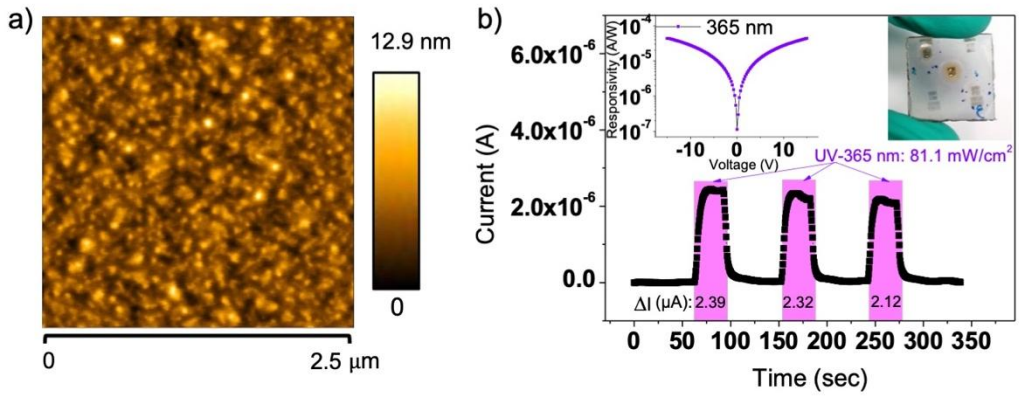

Fig. 6: An 808 nm laser annealed (a) Au NPs on photopolymerized resin substrate by 5.5 $W \cdot cm^{-2}$, 10 min, and (b) an Au NPs/IZO PD for UV (365 nm, 81.1 $mW \cdot cm^{-2}$) dynamic detection.

4. Conclusion

In this study, a novel solution-processed Au NPs/IZO PD with a wide range of detection performance, fabricated by an 808 nm laser annealing process, was successfully achieved. First, we recognized that the strong absorption of the Au film with a thickness of 8 nm in the NIR range could generate heat from 808 nm laser irradiation (28 $W \cdot cm^{-2}$, 30 min). Then, the Au NPs, which have similar morphology and absorption characteristics, could be successfully converted from a following annealing step. After IZO layer coupling with the 2nd annealing process (20 $W \cdot cm^{-2}$, 1 h), the basic dark current of the PD could be lowered by the disconnected structure

of Au NPs, which efficiently led to the improvement in light detection. The surface morphology of such nanocomposite structure was analyzed by spectroscopy, AFM TEM. Further structural characterization could be done later based on SEM or TEM cross-section imaging to better describe the interface between metal and semi-conductor. Besides, due to the hypothesis of the coupling of Au NPs cannot be neglected, we demonstrated the photosensitivity of IZO PDs with and without Au NP doping, utilizing commercial LEDs. Obviously, as IZO only has stronger absorption in the range < 400 nm, the addition of Au NPs can improve the absorption in a longer wavelength range (> 500 nm) owing to the LSPR effect. The generation of hot carriers not only improved the detection of green light (515 nm, ~5×10^{-3} $A \cdot W^{-1}$) but also extended the detection range to red (630 nm, ~5×10^{-4} $A \cdot W^{-1}$), and even to the NIR (780 nm, 10^{-4} $A \cdot W^{-1}$). The 808-nm-laser-annealed Au NPs/IZO PD offered good reliability and stability, performing with dynamic detection and keeping its operating lifetime for more than 22 d. Even though the high potential for use in solutions based on this technique has been performed, other kinds of MO functional nanostructure (ZnO:Cd- La, and TiO_2:Ni) **[60,61]** or thin film (TiO_2:Fe, ZnO:Al, and ZnO:Li) **[62-64]** composed from sol-gel network are still worth to be tested for optimizing the photoresponsivity or response speed. Furthermore, from our work, the initial trials of fabricating Au NPs/IZO PD on 3D printable polymer substrates for UV (365 nm) detection were accomplished under a low power 808-nm-laser-annealing process. In the near future, we aim to combine nanocomposite Au NPs/IZO or other sol-gel based metal oxide PD with colorimetric sensing techniques for building low-cost and reliable biomedical sensing systems.

Acknowledgement:

The authors would like to acknowledge the support of Agence Nationale pour la recherche (Project ANR-18-CE24-0028), Région Grand-Est and Institut Carnot MICA, Institute and Ministry of Science and Technology, Taiwan (Projects 108-2923-E-009 -002 -MY3) and the Higher Education Sprout Project of the National Chiao Tung University and Ministry of Education (MOE), Taiwan. We also gratefully thank Benjamin Leuschel, Samar Garreau, and Loic Vidal for their technical assistance.

References:

[1] C. C. Yeh, H. W. Zan & O. Soppera., Solution- Based Micro- and Nanoscale Metal Oxide Structures Formed by Direct Patterning for Electro- Optical Applications., Advanced Materials, 30(50), 1800923., (2018)

[2] A. Waseem, M. A. Johar, M. A. Hassan, I. V. Bagal, J. S. Ha, J. K. Lee & S. W. Ryu., Cu_2O Heterostructured GaN Thin Film and GaN Nanowire Piezoelectric Nanogenerators., physica status solidi (a), 217(7), 1900798., (2020)

[3] C. F. Lin, C. H. Kao, C. Y. Lin, K. L. Chen & Y. H. Lin., NH_3 Plasma-Treated Magnesium Doped Zinc Oxide in Biomedical Sensors with Electrolyte–Insulator–Semiconductor (EIS) Structure for Urea and Glucose Applications., Nanomaterials, 10(3), 583., (2020)

[4] C. Y. Chi, H. I. Chen, W. C. Chen, C. H. Chang & W. C. Liu., Formaldehyde sensing characteristics of an aluminum-doped zinc oxide (AZO) thin-film-based sensor., Sensors and Actuators B: Chemical, 255, 3017-3024., (2018)

[5] S. Abbas, M. Kumar, D. K. Ban, J. H. Yun & J. Kim., Transparent and Flexible In_2O_3 Thin Film for Multilevel Nonvolatile Photomemory Programmed by Light., ACS Applied Electronic Materials, 1(3), 437-443. (2019)

[6] M. Lee, W. Lee, S. Choi, J. W. Jo, J. Kim, S. K. Park & Y. H. Kim., Brain- Inspired Photonic Neuromorphic Devices using Photodynamic Amorphous Oxide Semiconductors and their Persistent Photoconductivity., Advanced Materials, 29(28), 1700951., (2017)

[7] F. Alema, B. Hertog, O. Ledyaev, D. Volovik, G. Thoma, R. Miller & W. V.

Schoenfeld., Solar blind photodetector based on epitaxial zinc doped Ga_2O_3 thin film., Physica status solidi (a), 214(5), 1600688., (2017)

[8] Ahmed, A. A., Hashim, M. R., Abdalrheem, R., & Rashid, M., High-performance multicolor metal-semiconductor-metal Si photodetector enhanced by nanostructured NiO thin film., Journal of Alloys and Compounds, 798, 300-310., (2019)

[9] D. Dong, W. Wang, G. Dong, F. Zhang, Y. He, H. Yu, F. Liu, M. Wang & X. Diao., Electrochromic properties and performance of NiOx films and their corresponding all-thin-film flexible devices preparedby reactive DC magnetron sputtering., Applied Surface Science, 383, 49-56., (2016)

[10] K. M. Niang, J. Cho, A. Sadhanala, W. I. Milne, R. H. Friend & A. J. Flewitt., Zinc tin oxide thin film transistors produced by a high rate reactive sputtering: effect of tin composition and annealing temperatures., physica status solidi (a), 214(2), 1600470., (2017)

[11] H. D. Dawoud, T. Al Tahtamouni & N. Bensalah., Sputtered manganese oxide thin film on carbon nanotubes sheet as a flexible and binder- free electrode for supercapacitors., International Journal of Energy Research, 43(3), 1245-1254., (2019)

[12] S. Y. Yu, G. Schrodj, K. Mougin, J. Dentzer, J. P. Malval, H. W. Zan, O. Soppera & A. Spangenberg., Direct Laser Writing of Crystallized TiO_2 and TiO_2/Carbon Microstructures with Tunable Conductive Properties., Advanced Materials, 30(51), 1805093., (2018)

[13] S. Y. Han, G. S. Herman & C. H. Chang., Low-temperature, high-performance, solution-processed indium oxide thin-film transistors., Journal of the American Chemical Society, 133(14), 5166-5169., (2011)

[14] K. Nomura, H. Ohta, A. Takagi, T. Kamiya, M. Hirano & H. Hosono., Room-temperature fabrication of transparent flexible thin-film transistors using amorphous oxide semiconductors., nature, 432(7016), 488-492., (2004)

[15] B. Leuschel, A. Gwiazda, W. Heni, F. Diot, S. Y. Yu, C. Bidaud, L. Vonna, A. Ponche, H. Haidara & O. Soppera., Deep-UV photoinduced chemical patterning at the micro-and nanoscale for directed self-assembly., Scientific reports, 8(1), 1-15. (2018)

[16] Y. M. Noor, S. C. Tam, L. E. N. Lim & S. Jana., A review of the Nd: YAG laser

marking of plastic and ceramic IC packages., Journal of materials processing technology, 42(1), 95-133., (1994)

[17] N. Ezra, A. Arshanapalli, R. Bednarek, S. Akaishi & A. K. Somani., The microsecond 1064 nm Nd: YAG laser as an adjunct to improving surgical scars following Mohs micrographic surgery., Journal of Cosmetic and Laser Therapy, 18(4), 225-229., (2016)

[18] Y. H. Kim, J. S. Heo, T. H. Kim, S. Park, M. H. Yoon, J. Kim, M. S. Oh, G. R. Yi, Y. Y. Noh & S. K. Park., Flexible metal-oxide devices made by room-temperature photochemical activation of sol–gel films., Nature 489, 128–132 (2012).

[19] S. Bolat, P. Fuchs, S. Knobelspies, O. Temel, G. T. Sevilla, E. Gilshtein, C. Andres, I. Shorubalko, Y. Liu, G. Tröster & Tiwari, A. N., Inkjet- Printed and Deep- UV- Annealed YAlOx Dielectrics for High- Performance IGZO Thin- Film Transistors on Flexible Substrates., Advanced Electronic Materials, 5(6), 1800843., (2019)

[20] C. J. Moon & H. S. Kim., Intense Pulsed Light Annealing Process of Indium–Gallium–Zinc–Oxide Semiconductors via Flash White Light Combined with Deep-UV and Near-Infrared Drying for High-Performance Thin-Film Transistors., ACS applied materials & interfaces, 11(14), 13380-13388., (2019)

[21] P. Y. Chang, C. F. Lin, S. El Khoury Rouphael, T. H. Huang, C. M. Wu, D. Berling, P. H. Yeh, C. J. Lu, H. F. Meng, H. W. Zan & O. Soppera., Near Infrared Laser–Annealed IZO Flexible Device as a Sensitive H2S Sensor at Room Temperature., ACS Applied Materials & Interfaces., (2020)

[22] J. A. Webb & R. Bardhan., Emerging advances in nanomedicine with engineered gold nanostructures., Nanoscale, 6(5), 2502-2530.3., (2014)

[23] J. H. Hodak, I. Martini & G. V. Hartland., Spectroscopy and dynamics of nanometer-sized noble metal particles., The Journal of Physical Chemistry B, 102(36), 6958-6967.3., (1998)

[24] S. Link, C. Burda, M. B. Mohamed, B. Nikoobakht & M. A. El-Sayed., Laser photothermal melting and fragmentation of gold nanorods: energy and laser pulse-width dependence., The Journal of Physical Chemistry A, 103(9), 1165-1170.3., (1999)

[25] S. Link & M. A. El-Sayed., Shape and size dependence of radiative,

non-radiative and photothermal properties of gold nanocrystals., International reviews in physical chemistry, 19(3), 409-453.3., (2000)

[26] L. R. Hirsch, R. J. Stafford, J. A. Bankson, S. R. Sershen, B. Rivera, R. E. Price, J. D. Hazle, N. J. Halas & J. L. West., Nanoshell-mediated near-infrared thermal therapy of tumors under magnetic resonance guidance., Proceedings of the National Academy of Sciences, 100(23), 13549-13554.3., (2003)

[27] A. O. Govorov, H. H. Richardson., Generating Heat with Metal Nanoparticles., Nano Today, 2 (1), 30–38.3., (2007)

[28] G. Baffou, F. Cichos, R. Quidant., Applications and challenges of thermoplasmonics., Nature Materials, 1-13.3., (2020)

[29] M. Fedoruk, M. Meixner, S. Carretero-Palacios, T. Lohmüller, J. Feldmann., Nanolithography by Plasmonic Heating and Optical Manipulation of Gold Nanoparticles., ACS Nano, 7 (9), 7648–7653., (2013)

[30] K. G. Stamplecoskie, C. Fasciani, J. C. Scaiano., Dual-Stage Lithography from a Light-Driven, Plasmon-Assisted Process: A Hierarchical Approach to Subwavelength Features. Langmuir, 28 (30), 10957–10961., (2012)

[31] J. M. Walker, L. Gou, S. Bhattacharyya, S. E. Lindahl, J. M. Zaleski., Photothermal Plasmonic Triggering of Au Nanoparticle Surface Radical Polymerization., Chemistry of Materials., 23 (23), 5275–5281., (2011)

[32] K. Matsumura, S. Toda & Y. Kato., RGB and Near-Infrared Light Reflectance/Transmittance Photoplethysmography for Measuring Heart Rate During Motion., IEEE Access, 8, 80233-80242., (2020)

[33] C. F. Lin, H. W. Zan, C. J. Lu, H. F. Meng & O. Soppera., A low-cost miniaturized colorimetric sensor with vertically-stacked semi-transparent finger-type organic photo detector for formaldehyde sensing., Organic Electronics, 73, 115-121., (2019)

[34] E. Monroy, F. Omnès & F. Calle., Wide-bandgap semiconductor ultraviolet photodetectors., Semiconductor science and technology, 18(4), R33., (2003)

[35] H. Zhu, Y. Fan, H. Guo, D. Huang & S. He., Reduced interhemispheric functional connectivity of children with autism spectrum disorder: evidence from functional near infrared spectroscopy studies., Biomedical optics express, 5(4), 1262-1274., (2014)

[36] S. Dias & S. B. Krupanidhi., Solution processed Cu_2SnS_3 thin films for visible

and infrared photodetector applications., AIP Advances, 6(2), 025217., (2016)

[37] H. Agarwal, S. V. Kumar & S. Rajeshkumar., A review on green synthesis of zinc oxide nanoparticles–An eco-friendly approach., Resource-Efficient Technologies, 3(4), 406-413. (2017)

[38] D. C. Paine, B. Yaglioglu,, Z. Beiley, & S. Lee., Amorphous IZO-based transparent thin film transistors., Thin solid films, 516(17), 5894-5898., (2008)

[39] J. Ye, D. Zuev & S. Makarov., Dewetting mechanisms and their exploitation for the large-scale fabrication of advanced nanophotonic systems., International Materials Reviews, 64(8), 439-477., (2019)

[40] M. Reddeppa, S. B. Mitta, T. Chandrakalavathi, B. G. Park, G. Murali, R. Jeyalakshmi, S.G. Kime, S. H. Park & M. D. Kim., Solution-processed Au@ rGO/GaN nanorods hybrid-structure for self-powered UV, visible photodetector and CO gas sensors., Current Applied Physics, 19(8), 938-945., (2019)

[41] C. L. Hsu, Y. H. Lin, L. K. Wang, T. J. Hsueh, S. P. Chang & S. J. Chang., Tunable UV-and visible-light photoresponse based on p-ZnO nanostructures/n-ZnO/glass peppered with Au nanoparticles., ACS applied materials & interfaces, 9(17), 14935-14944., (2017)

[42] J. R. Dunklin, G. T. Forcherio, K. R. Berry, and D. K. Roper., Gold Nanoparticle–Polydimethylsiloxane Thin Films Enhance Thermoplasmonic Dissipation by Internal Reflection., The Journal of Physical Chemistry C 118 (14), 7523-7531., (2014)

[43] Y. T. Yen, C. W. Chen, M. Fang, Y. Z. Chen, C. C. Lai, C. H. Hsu, Y. C. Wanga, H. Linb, C. H. Shenc, J. M. Shiehc, J. C. Hob & J. C. Ho,. Thermoplasmonics-assisted nanoheterostructured Au-decorated $CuInS_2$ nanoparticles: Matching solar spectrum absorption and its application on selective distillation of non-polar solvent systems by thermal solar energy. Nano Energy, 15, 470-478., (2015)

[44] S. Link & M. A. El-Sayed., Size and temperature dependence of the plasmon absorption of colloidal gold nanoparticles. The Journal of Physical Chemistry B, 103(21), 4212-4217., (1999)

[45] V. N. Rai, A. K. Srivastava, C. Mukherjee & S. K. Deb., Surface enhanced absorption and transmission from dye coated gold nanoparticles in thin films. Applied optics, 51(14), 2606-2615., (2012)

[46] G. Baffou, I. Bordacchini, A. Baldi & R. Quidant., Simple experimental procedures to distinguish photothermal from hot-carrier processes in plasmonics. Light: Science & Applications, 9(1), 1-16., (2020)

[47] A. O. Govorov & H. H. Richardson., Generating heat with metal nanoparticles. Nano today, 2(1), 30-38., (2007)

[48] A. O. Govorov, W. Zhang, T. Skeini, H. Richardson, J. Lee & N. A. Kotov., Gold nanoparticle ensembles as heaters and actuators: melting and collective plasmon resonances. Nanoscale Research Letters, 1(1), 84., (2006)

[49] G. Baffou, R. Quidant & C. Girard., Heat generation in plasmonic nanostructures: Influence of morphology. Applied Physics Letters, 94(15), 153109., (2009)

[50] P. Pattanasattayavong, S. Rossbauer, S. Thomas, J. G. Labram, H. J. Snaith & T. D. Anthopoulos., Solution-processed dye-sensitized ZnO phototransistors with extremely high photoresponsivity. Journal of Applied Physics, 112(7), 074507., (2012)

[51] X. Hu, Y. Dong, F. Huang, X. Gong & Y. Cao., Solution-processed high-detectivity near-infrared polymer photodetectors fabricated by a novel low-bandgap semiconducting polymer., The Journal of Physical Chemistry C, 117(13), 6537-6543., (2013)

[52] Y. J. Kim, C. E. Park & D. S. Chung., Interface engineering of a highly sensitive solution processed organic photodiode., Physical Chemistry Chemical Physics, 16(34), 18472-18477., (2014).

[53] C. A. Perini, A. J. Barker, M. Sala, A. Petrozza & M. Caironi., High speed solution-processed hybrid perovskite photodetectors with low dark current enabled by a low temperature metal oxide interlayer., Semiconductor Science and Technology, 33(9), 094004., (2018)

[54] F. Cao, W. Tian, B. Gu, Y. Ma, H. Lu & L. Li., High-performance UV–vis photodetectors based on electrospun ZnO nanofiber-solution processed perovskite hybrid structures., Nano Research, 10(7), 2244-2256., (2017)

[55] J. R. Manders, T. H. Lai, Y. An, W. Xu,, J. Lee, D. Y. Kim, G. Bosman & F. So., Low- Noise Multispectral Photodetectors Made from All Solution- Processed Inorganic Semiconductors., Advanced Functional Materials, 24(45), 7205-7210., (2014)

[56] S. W. Shin, K. H. Lee, J. S. Park & S. J. Kang., Highly transparent, visible-light

photodetector based on oxide semiconductors and quantum dots., ACS applied materials & interfaces, 7(35), 19666-19671., (2015)

[57] A. D. Mottram, Y. H. Lin, P. Pattanasattayavong, K. Zhao, A. Amassian, & T. D. Anthopoulos., Quasi two-dimensional dye-sensitized In_2O_3 phototransistors for ultrahigh responsivity and photosensitivity photodetector applications., ACS applied materials & interfaces, 8(7), 4894-4902., (2016).

[58] Z. haifei, H. Xie, Y. Yang, K. Wang, F. Zhao, W. Ye & W. Ni., Mapping Hot Electron Response of Individual Gold Nanocrystals on a TiO_2 Photoanode., Nano Letters., (2020)

[59] X. Zhang, Y. L. Chen, R. S. Liu & D. P. Tsai., Plasmonic photocatalysis., Reports on Progress in Physics, 76(4), 046401., (2013)

[60] B. A. Gozeh, A. Karabulut, A. Yildiz & F. Yakuphanoglu., Solar light responsive ZnO nanoparticles adjusted using Cd and La Co-dopant photodetector., Journal of Alloys and Compounds, 732, 16-24., (2018)

[61] M. Manzoor, A. Rafiq, M. Ikram, M. Nafees & S. Ali., Structural, optical, and magnetic study of Ni-doped TiO_2 nanoparticles synthesized by sol–gel method., International Nano Letters, 8(1), 1-8., (2018)

[62] F. Kara, M. Kurban & B. Coşkun., Evaluation of electronic transport and optical response of two-dimensional Fe-doped TiO_2 thin films for photodetector applications., Optik, 210, 164605., (2020)

[63] C. Kumar, B. K. Kushwaha, A. Kumar, D. K. Jarwal, R. K. Upadhyay, A. P. Singh & S. Jit., Fibrous al-doped ZnO thin film ultraviolet photodetectors with improved responsivity and speed., IEEE Photonics Technology Letters, 32(6), 337-340., (2020)

[64] X. Zhu, Q. Xie, H. Tian, M. Zhang, Z. Gou, S. He, P. Gu, H. Wu, J. Li & D. Yang., High photoresponse sensitivity of lithium-doped ZnO (LZO) thin films for weak ultraviolet signal photodetector., Journal of Alloys and Compounds, 805, 309-317., (2019)